[Short title + Author Name - P&H title] 32 (2024) 101898

HOSTED BY

Contents lists available at ScienceDirect

Saudi Pharmaceutical Journal

journal homepage: www.sciencedirect.com

Isolation of a novel isoprenylated phenolic compound and neuroprotective evaluation of *Dodonaea viscosa* extract against cerebral ischaemia–reperfusion injury in rats

Omer M. Almarfadi [a,*], Nasir A. Siddiqui [a], Abdelaaty A. Shahat [a], Omer I. Fantoukh [a], Ali A. El Gamal [a], Mohammed Raish [b], Ahmed Bari [c], Muzaffar Iqbal [c], Ali S. Alqahtani [a]

[a] Department of Pharmacognosy, College of Pharmacy, King Saud University, P.O. Box 2457, Riyadh 11451, Saudi Arabia
[b] Department of Pharmaceutics, College of Pharmacy, King Saud University, Riyadh 11451, Saudi Arabia
[c] Department of Pharmaceutical Chemistry, College of Pharmacy, King Saud University, Riyadh 11451, Saudi Arabia

ARTICLE INFO

Keywords:
Antioxidant
Dodonaea
Ischaemia
MCAO
Neuroprotective
Phenolic

ABSTRACT

Dodonaea *viscosa* grows widely in Saudi Arabia, but studies evaluating its neuroprotective activity are lacking. Thus, this study aimed to isolate and identify the secondary metabolites and evaluate the neuroprotective effects of D. viscosa leaves. The isolation and identification of phytochemicals were performed using chromatographic and spectroscopic techniques. The neuroprotective potential of the extract was evaluated against focal cerebral ischaemia–reperfusion injury in rat model. Neurobehavioural deficits in the rats were evaluated, and their brains were harvested to measure infarct volume and oxidative biomarkers. Results revealed the presence of three compounds: a novel isoprenylated phenolic derivative that was elucidated as 4-hydroxy-3-(3'-methyl-2'-butenyl) phenyl 1-O-β-D-apiosyl-(1''' → 6")- β-D-glucopyranoside (named Viscomarfadol) and two known compounds (isorhamnetin-3-O-rutinoside and epicatechin (4–8) catechin). Pre-treatment of the rats with the extract improved neurological outcomes. It significantly reduced neurological deficits and infarct volume; significantly reduced lipid peroxidation, as evidenced by decreased malondialdehyde levels; and significantly elevated antioxidant (superoxide dismutase, catalase, and glutathione) activities. These results indicate that *D. viscosa* is a promising source of bioactive compounds that can improve neurological status, decrease infarct volume, and enhance antioxidant activities in rats with cerebral ischaemic injury. Thus, *D. viscosa* could be developed into an adjuvant therapy for ischaemic stroke and other oxidative stress-related neurodegenerative disorders. Further investigations are warranted to explore other bioactive compounds in *D. viscosa* and evaluate their potential neuroprotective activities.

1. Introduction

Stroke is an acute neurodegenerative disorder in which impairment of the cerebral circulation leads to a focal or global impairment of brain function. It is the second leading cause of mortality and the third leading cause of disability worldwide (Owolabi et al., 2022). Stroke can be classified into two major types: ischaemic and haemorrhagic. Ischaemic stroke represents 80–85 % of all stroke cases. Although more severe, haemorrhagic stroke is less common than ischaemic stroke, accounting for 15–20 % of all stroke cases (Perna and Temple, 2015). Two distinct pathological areas are generated in brain ischaemia: ischaemic core and penumbra. The ischaemic core is characterized by cerebral blood flow reduction below critical thresholds, causing severe and irreversible damage. The penumbra is the area around the ischaemic core that can alternatively receive cerebral blood flow and is prone to reversible ischaemia–reperfusion injury. Penumbral cells remain alive depending on the occlusion time and reoxygenation period (Fifield and Vanderluit, 2020). Oxidative stress is an ischaemic stroke event that involves the production of reactive oxygen species (ROS) (Kamal et al., 2023). Hypoxia disturbs intracellular ion haemostasis, aggravates

* Corresponding author.
E-mail addresses: oalmarfadi@ksu.edu.sa (O.M. Almarfadi), nsiddiqui@ksu.edu.sa (N.A. Siddiqui), ashahat@ksu.edu.sa (A.A. Shahat), ofantoukh@ksu.edu.sa (O.I. Fantoukh), aelgamel@ksu.edu.sa (A.A. El Gamal), mraish@ksu.edu.sa (M. Raish), abari@ksu.edu.sa (A. Bari), muziqbal@ksu.edu.sa (M. Iqbal), alalqahtani@ksu.edu.sa (A.S. Alqahtani).

https://doi.org/10.1016/j.jsps.2023.101898

Available online 9 December 2023

mitochondrial dysfunction, and causes mitochondrial permeability transition pore formation that allows free radicals, such as oxygen free radicals, oxygen-derived radicals, and superoxide anion radicals, and pro-apoptotic factors, to enter the cytosol (Sarkar et al., 2019). The rapid restoration of blood flow enhances tissue oxygenation and generates a second burst of ROS production, resulting in reperfusion damage (Huang et al., 2023). Oxidative stress leads to protein deterioration, lipid peroxidation of the cell membrane, DNA deletion and mutation, and brain cell death (Jelinek et al., 2021). Indigenous antioxidant enzymes, such as superoxide dismutase, catalase, and glutathione peroxidase, exert antioxidant activities, but their antioxidant mechanisms may be overwhelmed by the ROS overproduction during post-acute cerebral ischaemia, potentiating oxidative stress and causing brain tissue injury (Shou et al., 2022).

Dodonaea viscosa is an evergreen woody shrub belonging to the Sapindaceae family. It was native to Australia but later became widespread throughout tropical regions. In Saudi Arabia, D. viscosa grows tremendously in the South-western and Eastern Provinces and Hijaz region (Siddiqui et al., 2023). It contains a wide range of phytochemicals, including flavonoids, terpenoids, saponins, sterols, phenolics, sugars, alkaloids, and tannins (Hossain, 2019). Several specific phytochemicals of *D. viscosa* exhibit biological activities. For instance, C-alkylated flavonol derivatives possess selective urease inhibitory activities that potentiate the healing rate of peptic ulcers (Faraz et al., 2019), and isoprenylated flavonol derivatives A–J, can inhibit peripheral glucose uptake (Zhang et al., 2012). Terpenoids, such as hautriwaic acid, exhibit anti-inflammatory activities (Salinas-Sánchez et al., 2015).

According to the literature, oxidative stress plays a significant role in ischemic stroke, Consequently, antioxidant drugs have the potential to alleviate oxidative stress in the brain induced by ischemia (Jelinek et al., 2021). In our previous study, we observed a substantial antioxidant activity in *D. viscosa* when compared to ascorbic acid using DPPH and ABTS scavenging assays (Almarfadi et al., 2022). Building on this observation, we have formulated our hypothesis: administering a methanolic extract of *D. viscosa* may effectively counteract MCAO-induced oxidative stress, providing neuroprotection against ischemia–reperfusion injury in a rat model. Furthermore, it's worth noting that *D. viscosa* is abundant in Saudi Arabia, yet comprehensive phytochemical and biological studies assessing its neuroprotective properties are currently lacking. Thus, this study aimed to isolate and identify secondary metabolites and evaluate the neuroprotective effect of the *D. viscosa* grown in Saudi Arabia. The results of this study can serve as a basis for developing herbal drugs with neuroprotective properties.

2. Materials and methods

2.1. Plant material

Aerial parts of *D. viscosa* were collected from the Herbal Garden Pharmacy College, King Saud University in September 2019. A voucher specimen (voucher #15787) was deposited in the Herbarium of Pharmacy, Department of Pharmacy, King Saud University, Riyadh, Saudi Arabia.

2.2. Extraction

Air-dried leaf samples (3 kg) were ground into coarse powder and extracted by macerating with 80 % methanol (8 L) several times until exhausted at room temperature. After solvent evaporation using a rotary evaporator, the dry extract (DVME, 1.1 kg) was divided into two parts: 750 g was subjected to successive partitioning with solvents of increasing polarity (*n*-hexane, chloroform, ethyl acetate, and *n*-butanol), and 350 g was stored for further woke. The solvents were evaporated to produce five dry fractions: *n*-hexane (3.3 g), chloroform (130.6 g), ethyl acetate (36.84 g), *n*-butanol (92.6 g), and the remaining aqueous fraction (164.7 g). Then, the dried fractions were transferred into separated glass containers and stored at − 20 °C until use.

2.3. Fractionation and isolation of active compounds

Part of the ethyl acetate fraction (15 g) was subjected to chromatography on a normal-phase silica gel column. Elution started with 100 % *n*-hexane, followed by *n*-hexane: chloroform (50:50, *v/v*), chloroform: methanol (90:10, *v/v*), and then 100 % methanol. The collected fractions (150 mL each) were pooled according to their TLC similarity behaviour using EtOAc: formic acid: AcOH: H_2O (30:0.8:1.2:8, *v/v/v/v*) as a mobile phase to obtain eight major sub-fractions (E-1–E-8). Sub-fraction E-8 (2.5 g) was re-chromatographed on a reversed-phase column. The column was gradually eluted, starting with H_2O: MeOH (70:30, *v/v*) as the mobile phase. Based on the TLC similarities, the collected fractions were merged into 12 (E-8. (1–12)) sub-fractions. Then, sub-fraction E-8.5 (201.8 mg) was purified again on a Sephadex LH20 column and eluted with H_2O: MeOH (10:90, *v/v*) to obtain three (E-8.5. (1–3)) sub-fractions according to TLC similarity. Sub-fraction E-8.5.2 showed one major spot on TLC with ($Rf = 0.30$) using $CHCl_3$: MeOH: formic acid (7:1:1, *v/v/v*) as the mobile phase. It afforded 75.3 mg of compound (DVE-4).

Sub-fraction E-7 (2 g) was re-chromatographed on an RP18 column and eluted gradually starting from H_2O: MeOH (90:10, *v/v*). According to their reversed-phase TLC similarities, the collected fractions were merged into six (E-7. (1–6)) (sub-fractions). Sub-fraction E-7.4 (70 mg) was eluted with H_2O: MeOH (70:30, *v/v*) and purified again on a Sephadex LH20 column that was eluted with methanol: dichloromethane (1:2, *v/v*) to obtain four sub-fractions E-7.4. (1–4) based on their TLC similarities. Sub-fraction E-7.4.1 showed one major spot on TLC ($Rf = 0.42$) using $ChCl_3$: MeOH (7:1, *v/v*) as the mobile phase, affording 54 mg of compound (DVE-9). Sub-fraction 2 (230.8 mg) was eluted with water: methanol (70:30 *v/v*) and re-chromatographed on a Sephadex LH20 column eluted with H_2O: MeOH (1:2) to obtain five sub-fractions (1–5) depending on their TLC similarity. Sub-fraction 5 showed one major spot on RP-TLC with ($Rf = 0.58$). H_2O: MeOH (60:40) was used as the mobile phase and afforded 14.4 mg of compound (DVE-10).

2.4. Spectroscopic instruments

Ultraviolet (UV) absorption spectra were obtained using a Shimadzu Corporation instrument (Kyoto, Japan). The various chemical functional groups of the isolated compounds were determined using Fourier transform infrared spectroscopy (FT-IR) (Shimadzu Corporation, Kyoto, Japan). The ^{1}H and ^{13}C NMR spectra were recorded on a Bruker AMX-500 spectrometer. The chemical shift values were expressed in (ppm) units using tetramethylsilane as the internal standard, and the coupling constant (J) was expressed in hertz (Hz). Spectroscopic-grade methanol-d_4 and DMSO-d_6 were used as solvents. Mass spectrometry was performed on a quadrupole time-of-flight mass spectrometer (Waters Corporation, Milford, MA, USA).

2.5. Neuroprotective evaluation

2.5.1. Experimental design

Twenty-four male rats were randomly divided into the following four equal groups (n = 6 each). Group I (Control group) received normal saline and underwent placebo surgery that did not involve middle cerebral artery occlusion (MCAO); Group II (MCAO group) was subjected to the MCAO procedure; Group III (MCAO + DVME group) received a pre-treatment of DVME at a dosage of 300 mg/kg administered orally; Group IV (DVME + MCAO group) received a pre-treatment of DVME at a dosage of 150 mg/kg administered orally. After 30 days of treatment period, 45 min MCAO was proceeded followed by 24 h of reperfusion before the rats were sacrificed. all procedures were performed in compliance with relevant laws and institutional guidelines and approved by the Research Ethics Committee of King Saud University.

2.5.2. Surgical procedure

MCAO induction was performed as previously described (Abdel-Rahman et al., 2020). Briefly, rats were anesthetized with zoletil® (tiletamine + zolazepam), at 80 mg/kg intraperitoneal ketamine and xylazine (10 mg/kg) injection. The body temperature was maintained throughout surgery (36.5–37.0 °C) by monitoring the rectal temperature. Surgery was performed to expose the right common carotid artery (CCA), internal carotid artery (ICA), and external carotid artery (ECA) was ligated, then A 4–0 nylon suture with a silicon tip was threaded through the ECA stump into the ICA, occluding the MCA at a distance of 18 to 22 mm from the place of insertion. At the end of 45 min of MCAO. The suture was removed to start reperfusion for 24 hrs; when the reperfusion was confirmed, the neck was stitched using surgical thread.

2.5.3. Evaluation of neurological status

The neurological scores of each rat were carefully evaluated after ischaemia–reperfusion and before sacrifice by using a grading scale of 0–4 as previously described (Shah et al., 2021).

The neurological score of each rat is evaluated carefully after ischemia, after reperfusion, and before sacrifice. Neurological score 0 indicated the animal remained normal, no abnormality; score 1 indicated Forelimb flexion and thorax twisting; score 2 states the animal is circling towards the contra-lateral side by pulling the tail and keeping the forelimb on the ground; Score 3 indicated spontaneous circling movement toward the contralateral side and score 4 indicated docile. This method was used to assess the effects of occlusion on neurological status.

2.5.4. Measuring the volume of the cerebral infarct

The cerebral infarct volume was determined by 2,3,5-triphenyltetrazolium chloride (TTC) as described by a previous study (Gupta et al., 2018). Briefly, rats were killed 24 h after reperfusion, and brains were rapidly removed and frozen at − 20 °C for 5 min. The brains were sliced into 2 mm thick coronal sections. The slices were placed in 2 % TTC at 37 °C for 20 min and the infarct volume was demarcated and analyzed using a digital camera (Canon EOS 400) and the software Adobe Photoshop 7.0. The infarct size was calculated with the Mias-2000 image analysis system (Institute of Image NIH). The corrected infarct volume was calculated to eliminate edema error: To compensate for the effect of brain edema, the corrected infarct volume was calculated as follows: corrected infarct area = measured infarct area {1- [(ipsilateral hemisphere area-contralateral hemisphere area)/contralateral hemisphere]. Infarcted areas of all sections were added to derive the total infarct area, which was multiplied by the thickness of the brain sections to obtain the infarct volume.

2.6. Estimation of oxidative stress biomarkers MDA, SOD, CAT, and GSH

MDA, SOD, CAT, and GSH were detected using the ELISA kits (No. ab83464, ab65354, ab118970, and ab239727), respectively. Briefly, MDA in the brain tissue reacts with thiobarbituric acid (TBA) to generate an MDA–TBA complex which is detected and quantified at a specific absorption at 532 nm. For SOD, brain tissues were incubated (at 37 °C for 30 min) with a WST-8/enzyme working solution. The absorption was detected at a wavelength of 450 nm. For CAT, brain tissues were mixed with CAT assay buffer and H_2O_2 solution. After incubating for 5 min at 25 °C, the absorption was measured at a wavelength of 520 nm. For GSH, brain tissues were mixed with GSH at 37 °C for 5 min. After centrifugation, The absorption of supernatant was detected at a wavelength of 412 nm (An et al., 2022).

2.7. Statistical analysis

Data obtained from animal experiments were expressed as the mean and standard error of the mean (mean ± SEM). Statistical differences between the control and treated groups were evaluated through one-way ANOVA and post-hoc Tukey's test using GraphPad Prism-8 software. In all cases, $P < 0.05$ was considered to indicate statistical significance.

3. Results

3.1. Isolation and structure characterization of phytochemicals

DVE-9 was isolated from EtOAc fraction as a white amorphous powder with a weight of 54.2 mg. The structure of DVE-9 was elucidated by spectroscopic methods (UV, FT-IR, 1D and 2D NMR, and LC-MS). UV (MeOH) showed λ max 287 nm and 225 nm (supplementary file, Fig. 2). FT-IR (KBr) exhibited *ν* max 3429 cm^{-1}, 2924 cm^{-1}, 1649 cm^{-1}, 1440 cm^{-1} and 1060 cm^{-1} (supplementary file, Fig. 3). ^{1}H NMR (700 MHz, DMSO): $\delta = 8.90$ (*s*, 1H, 4-OH), 6.70 (*dd*, $J = 8.6, 2.8$, 1H, H-6), 6.68 (*d*, $J = 2.8$ Hz, 1H, H-2), 6.66 (*d*, $J = 8.6$ Hz, 1H, H-5), 5.25 (*m*, 1H. 4"-OH), 5.23 (*d*, $J = 5.2$, 1H, H-2'), 5.07 (*t*, $J = 5.6$, 1H, 3"-OH), 5.01 (*d*, $J = 6.4$, 1H, 2"-OH), 4.82 (*d*, $J = 3.0$ Hz, 1H, H-1'"), 4.74 (*t*, $J = 5.7$ Hz, 1H, 5'"-OH), 4.58 (*d*, $J = 7.8$ Hz, 1H, H-1"), 4.49 (*s*, 1H, 3'"-OH), 3.86 (*d*, $J = 9.4$, 1H,H-4'"a), 3.84 (*d*, $J = 11.1$, 1.3 1H, H- 6"a), 3.73 (*d*, $J = 6.4$, 3.0, 1H, H-2'"), 3.58 (*d*, $J = 9.3$, 1H, H-4'"b), 3.42 (*dd*, $J = 11.0$, 6.7, 1H, H-6"b), 3.38 (*dd*, 9.5, 1.51H, H-5"), 3.36 (*brd*, $J = 5.8$, 1H, H-5'"a), 3.34 (*brd*, $J = 5.8$, 1H, H-5'"b), 3.20 (*dd*, $J = 8.9$, 5.0 1H, H-3"), 3.16 (*d*, $J = 5.3$, 1H, H-1'), 3.15 (*m*, 1H, H-2"), 3.08 (*dd*, $J = 9.3$, 5.6 1H, H-4"), 1.69 (*s*, 3H, H-5'), 1.65 (*s*, 3H, H-4') ppm; ^{13}C NMR (176 MHz, DMSO): $\delta = 150.31$ (C-1), 149.7 (C-4), 131.4 (C-3'), 128.1(C-3), 122.7 (C-2'), 118,0 (C-2), 115.0 (C-5), 114.2 (C-6), 109.3 (C-1'"), 101.6 (C-1"), 78.8 (C-3'"), 76.6 (C-3"), 76.0 (C-2'"), 75.4 (C-5"), 73.3 (C-4'"), 73.2 (C-2"), 69.9 (C-4"), 67.5 (C-6"), 63.3 (C-5'"), 28.0 (C-1'), 25.5 (C-5'), 17.6 (C-4') ppm (supplementary file, Figs. 4-10). LC-MS/MS showed a molecular ion peak at *m/z* 471.21 $[M-H]^-$ and significant fragmentation peaks at *m/z* 292.98, 232.90 and 148.86 (supplementary file, figure 23–25).

DVE-4 was isolated from EtOAc fraction as pale yellowish crystals; weight (75.3). The structure of DVE-4 was elucidated by spectroscopic methods (UV, FT-IR, 1D and 2D NMR, and LC-MS). UV (MeOH) sowed at λ max 356 nm (band 1) and 254 nm (band 2) (supplementary file, Fig. 2). FT-IR (KBr) exhibited *ν* max 3445 cm^{-1}, 2927 cm^{-1}, 1651 $cm^{-1}$and 1610 cm^{-1} (supplementary file, Fig. 3). ^{1}H NMR (700 MHz, MeOD-d): $\delta = 8.02$ (d, $J = 2.0$ Hz, 1H, H-2), 7.59 (dd, $J = 8.40$, 2.0 Hz, 1H, H-6), 6.90 (d, $J = 8.40$ Hz, 1H, H-5), 6.38 (d, $J = 2.0$ Hz, 1H, H-8), 6.19 (d, $J = 2.0$ Hz, 1H, H-6), 5.20 (d, $J = 7.81$ Hz, 1H, H-1), 4.87 (s, 1H, OH), 4.52 (d, $J = 1.30$ Hz, 1H, H-1), 3.95 (*s*, 1H,), 3.94 (s, 1H, OCH_3), 3.82 (dd, $J = 9.6, 7.9$ Hz, 1H, H-2), 3.78 (d, $J = 3.3$ Hz, 3H), 3.74 (dd, $J = 10.3, 5.6$ Hz, 3H), 3.65 (t, $J = 6.3$ Hz, 3H), 3.59 – 3.55 (m, 6H), 3.54 – 3.51 (m, 3H), 3.49 (dd, $J = 9.5, 3.4$ Hz, 3H), 3.45 (dd, $J = 10.2, 6.9$ Hz, 3H), 3.34 (s, 17H), 3.30 (dt, $J = 3.2, 1.6$ Hz, 13H), 3.27 (t, $J = 9.5$ Hz, 3H), 1.17 (d, $J = 6.2$ Hz, 3H, H-6) ppm; ^{13}C NMR (176 MHz, MeOD-*d*): $\delta = 179.38$(C-4), 166.93(C-7), 162.97(C-5), 158.76(C-9), 158.55(C-2), 150.88(4), 148.40 (3), 135.46(3), 123.75(C-1), 122.97(6), 115.98(C-5), 114.59(C-2), 105.43(C-10), 105.00(C1), 101.92(C1), 100.23(C-6), 95.05(C-8), 70.03 –75.50(Oxy carbons of glycone part), 69.71(C-6), 67.41(C-5), 56.93 (–OCH_3), 17.97(C-6) ppm (supplementary file, figure 11–16). LC-MS/MS spectrum exhibited a strong peak at *m/z* 623.14 and significant fragmentation peaks at *m/z* 315.02 and 298.78 (supplementary file, figure 23–24, 26).

DVE-10 was isolated from EtOAc fraction as a yellow-colored powder; Weight (14.4) mg. Its structure was elucidated by spectroscopic methods UV, FT-IR, 1D and 2D NMR and LC-MS. UV (MeOH) showed λ max at 281 nm (band 1) and 213 nm (band 2) (supplementary file, Fig. 2). FT-IR (KBr) exhibited *ν* max at 3422 cm^{-1}, 2910 cm^{-1} and 1610 cm^{-1} (supplementary file, Fig. 3). ^{1}H NMR (700 MHz, DMSO) upper unit: $\delta = 6.79$ (*brs,* 2H, H-2 /H-6), 6.51 (*d*, $J = 7.5$ Hz, 1H, H-5), 5.81 (*s*, 1H, H-8), 5.71 (*s*, 1H, H-6), 4.94 (*s*, 1H, H-2), 4.44 (*d*, $J = 4.1$,1H, H-4), 3.62 (*s*, 1H, H-3), 8.76 (*s*, 1H, OH-4), 8.67 (*s*, 1H, OH-3), 8.63 (*s*, 1H, OH-5), 8.06 (*s*, 1H, OH-7), 4.29 (*s*, 1H, OH-3) ppm. Lower unit: $\delta = 6.99$ (*s,* 1H, H-2), 6.61 (*d*, $J = 8.1$, 1H, H-5), 6.63 (*d*, $J = 8.2$, 1H, H-6), 5.81 (*s*,

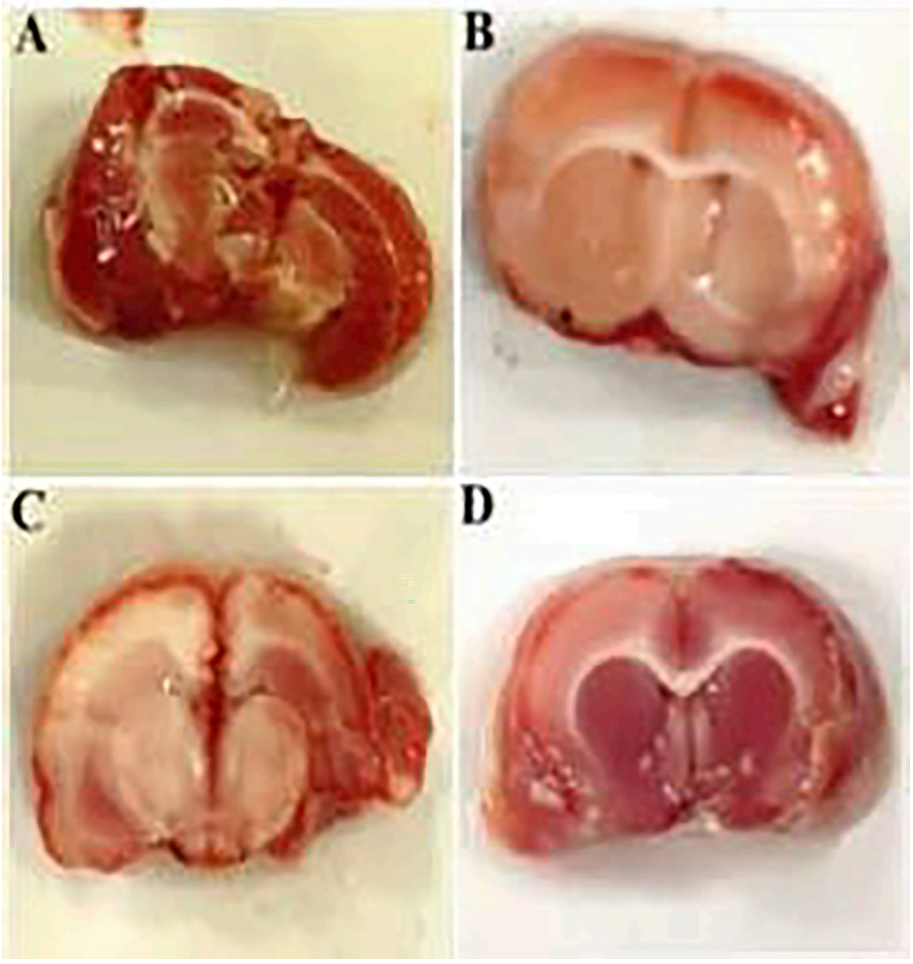

Fig. 1. Effect of *D. viscosa* methanolic extract on cerebral infarct volume in rats after cerebral occlusion ischaemia. (A) TTC staining exhibits red staining in the hemisphere of control rats. (B) TTC staining exhibits no red staining in the left hemisphere of ischaemic brain. (C) TTC staining exhibits that treatment with *D. viscosa* methanolic extract (150 mg/kg) mildly prevents ischaemia in the left hemisphere of ischaemic brain, and (D) TTC staining exhibits that treatment with *D. viscosa* methanolic extract (300 mg) moderately prevents ischaemia in the left hemisphere of ischaemic brain. (For interpretation of the references to colour in this figure legend, the reader is referred to the web version of this article.)

1H, H-8), 5.78 (*s*, 1H, H-6), 4.90 (*s*, 1H, H-2), 4.16 (*s*, 1H, H-3), 2.36 (*d*, $J = 12.3$, 1H, H-4a), 2.70 (*d*, $J = 12.8$,1H, H-4b), 8.91(*s*, 1H, OH-5), 8.76 (*s*, 1H, OH-4), 8.36 (*s*, 1H, OH-3), 7.99 (*s*, 1H, OH-7), 4.75 (*s*, 1H, OH-3) ppm; ^{13}C NMR (176 MHz, DMSO-d_6) Upper unit: $\delta = 156.6$ (C-9), 155.6 (C-7), 153.9 (C-5), 144.3 (C-2), 144.0 (C-4), 130.3 (C-1), 117.7 (C-5, C-6), 101.9 (C-10), 95.8 (C-8), 93.7 (C-6), 75.4 (C-2), 71.4 (C-3), 35.6 (C-4) ppm. Lower unit: $\delta = 155.9$ (C-7), 154.5 (C-5), 152.9 (C-9), 144.6 (C-3), 144.2 (C-4), 131.2 (C-1), 114.9 (C-5, C-6), 114.4 (C-2), 107.1 (C-8), 98.7 (C-10), 94.6 (C-6), 77.4 (C-2), 64.7 (C-3), 27.6 (C-4) ppm (supplementary file, figure 17–22). LC-MS/MS showed a molecular ion peak at *m/z* 577.08 [M−H and significant fragmentation peaks at *m/z* 407.04, 288.78 and 244.99 (supplementary file, figure 23, 24, 27).

3.2. Neurological deficit and infarct volume

Neurological deficits and infarct volume were significantly increased in the MCAO group compared with the control group ($P < 0.05$). MCAO-induced neurological deficits and brain infarct volume were significantly attenuated in the DVME-pre-treated groups (150 and 300 mg/kg/day) in a dose-dependent manner compared with the MCAO group ($P < 0.05$). Neurological function improved by 27.27 % and 54.55 %, respectively, whereas infarct volume was reduced by 25.79 % and 45.26 %, respectively, at both low and high doses in the DVME pre-treatment groups compared with the MCAO group (Figs. 1, 2a, 2b).

3.3. Oxidant stress biomarkers

The MDA level in the brain was measured 24 h after MCAO. It was significantly higher ($P < 0.05$) in the MCAO group than in the control group. Meanwhile, the MDA level was significantly lower ($P < 0.05$) in the DVME-pre-treated groups (150 and 300 mg/kg) than in the MCAO group by approximately 16.14 % and 37.04 %, respectively (Fig. 2c). The SOD activity in the ischaemic region was significantly lower ($P < 0.05$) in the MCAO group than in the control group. Meanwhile, the SOD activity was significantly higher ($P < 0.05$) in the DVME-pre-treated groups (150 and 300 mg/kg) than in the MCAO group by approximately 83.49 % and 122.58 %, respectively (Fig. 2d). The CAT activity was significantly lower in the MCAO group than in the control group ($P < 0.05$). Meanwhile, the CAT activity was significantly higher ($P < 0.05$) in the DVME-pre-treated groups (150 and 300 mg/kg) than in the MCAO group by approximately 78.04 % and 138.26 %, respectively (Fig. 2e). The GSH level in the brain was significantly depleted after the induction of focal cerebral ischaemia in rats. It was significantly lower in the MCAO group than in the control group ($P < 0.05$). Meanwhile, the GSH level was significantly higher ($P < 0.05$) in the DVME-pre-treated (150 and 300 mg/kg) groups than in the MCAO group by approximately 28.19 % and 69.12 %, respectively (Fig. 2f).

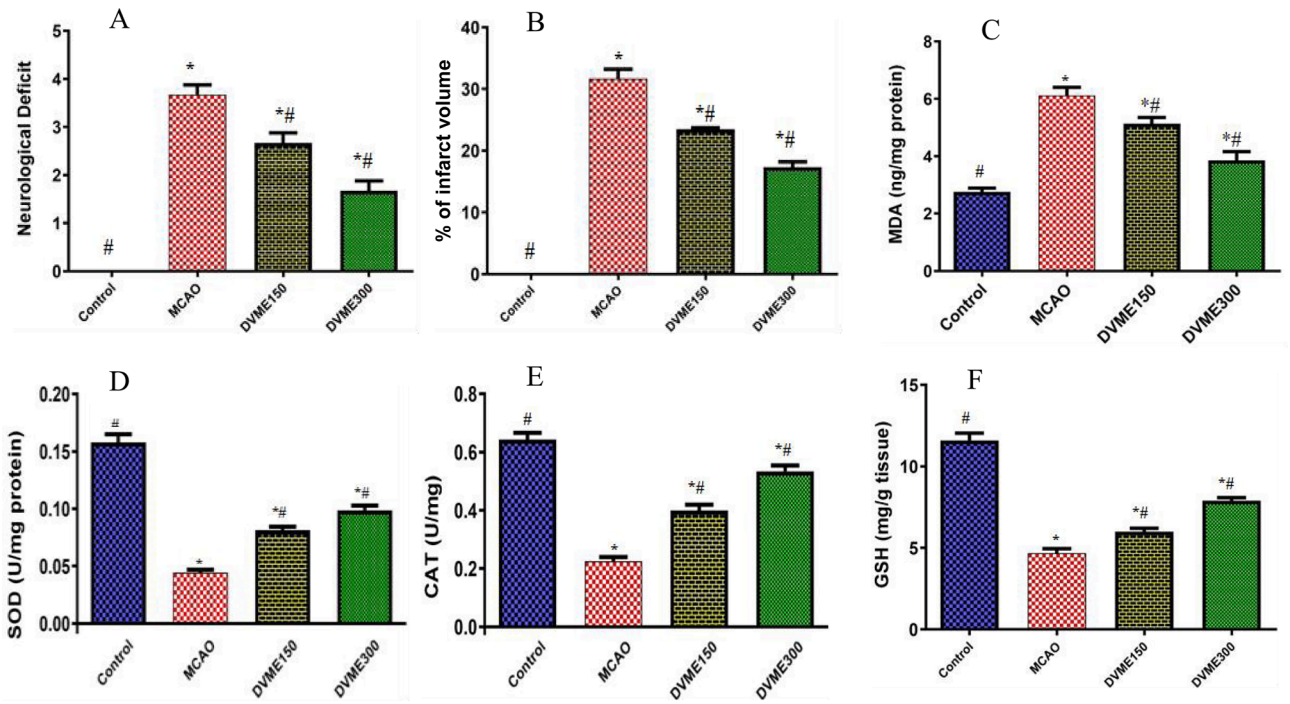

Fig. 2. Effects of DVME on (A) neurological deficient score, (B) infarct volume, (C) MDA level, (D) SOD level, (E) CAT level, and (F) GSH level in the brain of different groups. Statistical analysis was performed using one-way ANOVA followed by a post-hoc Tukey test. Values represent means ± (SEM) of each group, *P < 0.05 compared with the normal group, #P < 0.05 compared with the MCAO group.

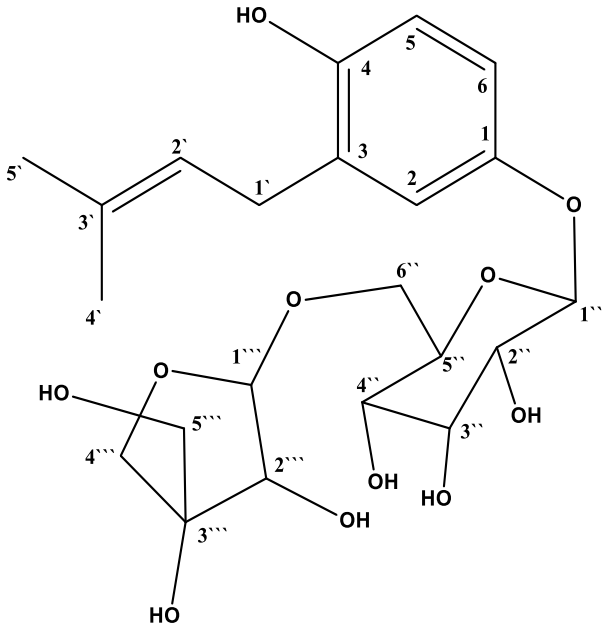

Fig. 3. Chemical structure of compound DVE-9.

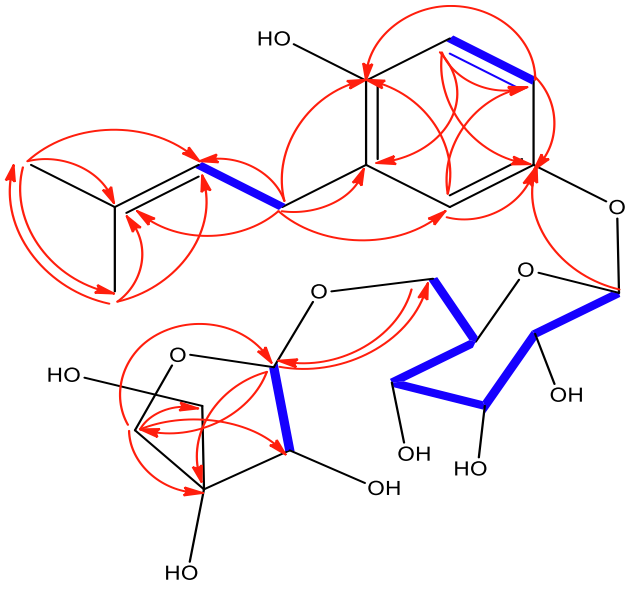

Fig. 4. COSY (blue) and HMBC (red) of compound DVE-9. (For interpretation of the references to colour in this figure legend, the reader is referred to the web version of this article.)

4. Discussion

4.1. Characterization of isolated compounds

In this study, a dual solvent mixture has been used to improve the solubility and promote the interaction of the targeted analyte with the extraction solvent enhancing the extraction yield (Radzali et al., 2020). The total extract was subjected to successive partition with organic solvents of increasing polarity (n-hexane, chloroform, ethyl acetate, and n-butanol). Depending on the TLC profile, The EtOAc fraction was selected for the isolation of phytoconstituents using column chromatography with different stationary phases which involve normal-phase silica, reversed-phase silica and Sephadex L20. In this work three pure compounds have been obtained. The structure elucidation of these compounds has been determined by various spectroscopic techniques which involve UV, FT-FT-IR, 1D and 2D NMR and LC-MS.

DVE-9: The ultraviolet spectrum showed λ max at 287 and 225 nm, which corresponded to the aromatic ring and aliphatic side chain. FT-IR spectrum showed a broad absorption band at 3429 cm^{-1}, which corresponded to a hydroxyl group, as confirmed by the C-O absorption band

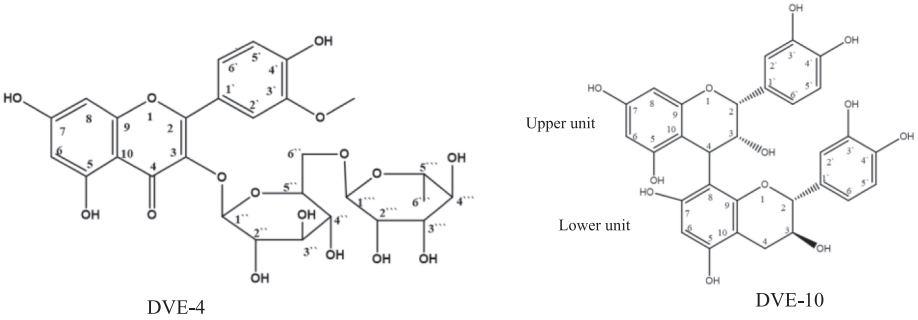

Fig. 5. Chemical structure of compound of DVE-4 and DVE-10.

at 1060 cm^{-1}. The absorption band at 2924 cm^{-1} indicated a methyl group, and the medium absorption at 1649 and 1440 cm^{-1} corresponded to the presence of an aromatic ring. The ^{1}H NMR spectrum showed resonances for three coupled aromatic proton signals at δ_H 6.68 (*d*, $J = 2.8$ Hz, 1H, H-2), 6.70 (*dd*, $J = 8.6$, 2.8 Hz, 1H, H-6), and 6.56 (*d*, $J = 8.6$ Hz, 1H, H-5), suggesting the presence of a 1,3,4-trisubstituted aromatic ring. Moreover, it showed other signals for tri-substituted vinyl group proton at δ_H 5.23 (*d*, $J = 5.2$ Hz, 1H, H-2'), aliphatic proton signals at δ_H 3.16 (*d*, $J = 5.3$ Hz, 2H, H-1'), and two olefinic methyl groups 1.66 (*s*, 3H, H-4') and 1.69 (*s*, 3H, H-5') that indicate the presence of 3,3-dimethylallyl (prenyl) side chains. The ^{1}H NMR spectrum also showed two distinct signals for anomeric protons, a hexose anomeric proton resonance at δ_H 4.58 (*d*, $J = 7.8$ Hz, 1H, H-1") and a pentose proton resonance at δ_H 4.82 (*d*, $J = 3.0$ Hz,1H, H-1'"), indicating the presence of two sugars with the β-configuration of anomeric protons based on their coupling constant (Glc: $J = 7.8$ Hz; Api: $J = 3.0$ Hz). Thus, one of the sugars was distinguished as a β-D-glucose unit in the pyranose form, whereas the other was assigned as an β-D-apiose moiety (Zhang et al., 2017). The ^{13}C NMR spectrum displayed 22 carbon signals that were further differentiated by DEPT and HSQC to 5 quaternary carbons comprising two aromatic carbons at δ_C 122.7 (C-2') and 131.4 (C-3'), two oxygenated aromatic carbons at δ_C 150.3 (C-1) and 149.7 (C-4), and one oxygenated carbon at δ_C 78.8 (C-3'"); 11 methine carbons including seven oxygenated methines of a sugar moiety, 1 methine of prenyl side chain and 3 aromatic methine; 4 methylenes involving three oxygenated methylenes of a sugar moiety and 1 olefinic methylene of prenyl side chain; and 2 olefinic methyles of prenyl side chain. The spectroscopic data of DVE-9 were mostly similar to those of nebrodenside A, a phenolic glycoside previously isolated from *D. viscosa* (Khan et al., 2019), except for the presence of an apiose moiety showing proton resonance at δ_H 4.82 (*d*, $J = 3.0$ Hz, 1H, H-1'"), 3.73 (*q*, $J = 6.4$, 3.0 Hz, 1H, H-2'"), 3.58 (*d*, $J = 9.3$, H-4'"a), 3.86 (*d*, $J = 9.4$, IH, H-4'"b), 3.34 (*brd*, $J = 5.8$, 1H, H-5'"a), and 3.36 (*brd*, $J = 5.8$, 1H, H-5'"b). Moreover, LC-MS/MS showed a molecular ion peak at *m/z* 471.21 $[M-H]^-$, which was consistent with the molecular weight of 472. In addition, the LC-MS/MS fragmentation spectrum revealed a molecular ion peak for the parent compound at *m/z* 471.48 $[M-H]^-$ and other significant fragments at *m/z* 292.98 $[C_{16}H_{21}O_5^{3\bullet}]^-$, 232.90 $[C_{14}H_{17}O_3^{3\bullet}]^-$, and 148.86 $[C_5H_9O_5]^-$, which were calculated using the $C_{22}H_{32}O_{11}$ formula involving seven degrees of unsaturation (Supplementary File, Figs. 24–26). Based on these data, along with a comparison with the literature, the structure of DVE-9 was determined as 4-hydroxy-3-(3'-methyl-2'-butenyl) phenyl 1-*O*-β-D -apiosyl-(1'"→6")-β-D –glucopyranoside, named Viscomarfadol. It was isolated for the first time from a natural source and identified as a novel compound (Figs. 3 and 4).

DVE-4 and DVE-10 were identified as isorhamnetin-3-*O* –rutinoside (Fig. 5) and procyanidin B1 (epicatechin-(4, 8)-catechin) (Fig. 5), respectively. By comparing with the literature, these phytoconstituents are known compounds. They were isolated and characterized previously from several plants (Ilhan et al., 2019, Otify et al., 2019). However, in this study, they were isolated for the first time from *D. viscosa.*

4.2. Neuroprotective activity

Cerebral ischaemic stroke is a life-threatening brain disease. However, effective neuroprotective therapies for the acute phase of this disease are lacking. Thus, exploring safe and effective neuroprotective drugs is essential to solve this problem. Previous studies used the MCAO method to induce focal cerebral ischaemia in experimental rats. Post-ischaemia–reperfusion restores blood flow to ischaemic brain tissues associated with the generation of ROS, which cause destructive oxidative stress in cerebral cells (Zhang et al., 2022). In the present study, DVME exerted its neuroprotective effects by improving the neurological deficit score, reducing the cerebral infarct volume, and counteracting oxidative stress in ischaemia–reperfusion cerebral injury.

Bioactive herbs may protect the brain against ischaemic stroke by thwarting the destructive mechanisms associated with the ischaemic cascade, such as oxidative stress and inflammation. ROS overproduction generates detrimental oxidative stress and, when combined with the depletion of endogenous antioxidants, leads to neural damage and dysfunction. Many medicinal herbs that can counteract these harmful effects may protect against ischaemic stroke (Jittiwat et al., 2021). Previous studies used MCAO to induce acute focal cerebral ischaemia and evaluate the preventive effects of herbal drugs against cerebral injury in the animal model. MCAO increases ischaemia-induced oxidative stress in the brain and sustains the effectiveness of indigenous antioxidants (Shou et al., 2022). In the present study, we established that DVME protected against cerebral ischaemic injury by contracting neurological deficits and lowering brain infarct size in rats subjected to transient MCAO. Morphometric and neurological behavioural measurements are used to estimate the infarct volume and neurological deficits, representing qualitative and quantitative methods for determining the extent of ischaemia-induced brain injury (Wang et al., 2018). Neurological deficits and infarct volumes are indicators commonly used to evaluate the efficacy of neuroprotective agents in vivo (Peng et al., 2019). In the present study, the MCAO group exhibited marked neurological deficit deterioration and infarct volume elevation compared with the control group. By contrast, the infarct volume significantly decreased in the DVME-pre-treated groups compared with the MCAO group in a dose-dependent manner. This improvement may be attributed to bioactive compounds, such as flavonoids and phenolics, with antioxidant, anti-inflammatory, and anti-apoptotic properties that protect brain tissue against MCAO insult (Fan et al., 2021).

In addition, our study demonstrated the potential neuroprotective activity of DVME by optimizing the antioxidant activity in the brains of rats with focal cerebral ischaemia. The MDA levels in the brains of the treated groups decreased after ischaemia–reperfusion, whereas the levels of other antioxidant markers (SOD, CAT, and GSH) increased. MDA is a product of unsaturated fatty acid degradation in cell membranes exposed to oxidative stress (Althurwi et al., 2022). Therefore, MDA level is a potential biomarker of lipid peroxidation (oxidative damage) generated by free radicals, such as hydrogen peroxide (Lan et al., 2020). ROS reduce unsaturated fatty acids in the cell membrane,

consequently damaging neuronal and non-neuronal cells in the brain (Heidari et al., 2021). In the present study, after 24 h of MCAO, the MDA levels in the brain were more than double in the MCAO group compared with the control group, indicating oxidative stress; by contrast, the MDA levels in the DVME pre-treated groups significantly decreased in the ischaemic region, in a dose-dependent manner (Shi et al., 2021). This result clearly established that DVME components exert neuroprotective effects by attenuating ROS-induced lipid peroxidation, consistent with the findings of a previous study (Tseuguem et al., 2019).

SOD is an antioxidant enzyme that counteracts oxidative stress by eliminating O_2. SOD protects neural cells against injury induced by oxygen radical species (Alatawi et al., 2018). In the present study, the SOD level was significantly lower 24 h after MCAO in the MCAO group compared with the control group, whereas the SOD levels in the DVME pre-treated groups significantly increased in a dose-dependent manner. This result indicated that DVME protected the cerebral cells against MCAO-induced injury, which agrees with the result of a previous study (Althurwi et al., 2022). CAT is an antioxidant enzyme that plays an important role in the detoxification of H_2O_2 and protects cells against oxidative stress (Nandi et al., 2019). A previous study has reported that CAT levels decline in the ischaemic regions of experimental animals exposed to induced brain ischaemia (Shi et al., 2021). Also, in the present study, the CAT level in the ischaemic region was significantly lower in the MCAO group than in the control group. Meanwhile, the CAT levels in the DVME pre-treated groups significantly increased in a dose-dependent manner, consistent with the findings of a previous study (Dai et al., 2018). These results suggest that DVME exerts neuroprotection against the deleterious effects of oxidative stress in the ischaemic/reperfused brain by elevating CAT levels.

GSH is a sulfhydryl (SH) containing a non-enzymatic antioxidant molecule with free radical-scavenging activity (Raj et al., 2021). A previous study reported that GSH levels decrease in the brains of experimental animals with focal cerebral ischaemia conjugated with elevated cerebral infarct volume. However, pre-treatment with GSH synthase markedly elevates GSH levels which is associated with a reduction of infarct volume, suggesting a protective effect against MCAO (Liang et al., 2022). Similarly, the GSH level, in this work, was significantly lower in the MCAO group after 24 h of induced brain ischaemia than in the control group, while the GSH levels significantly increased in a dose-dependent manner in the DVME pre-treatment groups. This result suggests that DVME exerts antioxidant activity and protects brain cells against oxidative stress by increasing GSH levels.

ROS are produced in high amounts during cerebral ischaemia, accompanied by destructive oxidative stress, particularly during the MCAO phase, which exacerbates cerebral injuries (Zhang et al., 2022). Therefore, preventing ROS-induced oxidative stress, lowering ROS levels, or both are used as a therapeutic strategy to protect brain tissue against the harmful effects of ROS in post-cerebral ischaemia. A previous study reported the scavenging activity of *D. viscosa* against DPPH radicals (Almarfadi et al., 2022). In the present study, DVME protected against oxidative stress associated with transient brain ischaemia. Oral pre-treatment with DVME for 30 days exerted neuroprotection by increasing the activities of cellular antioxidants (SOD, CAT, and GSH) that protect against oxidative stress, which plays a crucial role in the aetiopathogenesis of ischaemic stroke. The antioxidant activity of DVME can be attributed to its phytochemical components, such as flavonoids and phenolics. These findings are consistent with previous findings that *D. viscosa* extract exhibits antioxidant effects (Hossain, 2019). The flavonoids and phenolics possibly exerted their antioxidant activities by scavenging free radicals and inhibiting lipid peroxidation, protecting the mitochondria and other brain cell components, and maintaining the normal function of endogenous antioxidants, such as SOD, CAT, and GSH.

5. Conclusion

One novel isoprenylated phenolic compound and two flavonoid compounds were isolated from *D. viscosa* leaves and then characterized using UV, FT-IR, NMR, and MAS spectroscopy. These compounds were thought to be responsible for the biological activities of this plant. *D. viscosa* exerted neuroprotective effects against cerebral ischaemia–reperfusion injury in the MCAO model by reducing the MDA level and enhancing the activities of endogenous antioxidants, including SOD, CAT, and GSH. The extract decreased the neurological deficits and infarct volume. The results of this study suggest that D. viscosa could be used as an adjuvant therapy for ischaemic stroke and other oxidative stress-related disorders, such as neurodegenerative diseases. Further phytochemical and biological investigations are warranted to explore other bioactive compounds and neurological activities of D. viscosa.

CRediT authorship contribution statement

Omer M. Almarfadi: Writing – review & editing, Investigation, Methodology, Conceptualization, Writing – original draft. **Nasir A. Siddiqui:** Writing – review & editing, Investigation, Conceptualization. **Abdelaaty A. Shahat:** Writing – review & editing, Investigation, Methodology, Conceptualization. **Omer I. Fantoukh:** Funding acquisition. **Ali A. El Gamal:** Investigation. **Mohammed Raish:** Methodology. **Ahmed Bari:** Methodology. **Muzaffar Iqbal:** Methodology. **Ali S. Alqahtani:** Investigation.

Declaration of Competing Interest

The authors declare that they have no competing financial interests or personal relationships that may have influenced the work reported in this study.

Acknowledgments

The Authors are thankful to the Researchers Supporting Project number (RSP2023R430), King Saud University, Riyadh, Saudi Arabia.

Funding

This research was funded by the Researchers Supporting Project (RSP2023R430), King Saud University, Riyadh, Saudi Arabia

Appendix A. Supplementary material

Supplementary data to this article can be found online at https://doi.org/10.1016/j.jsps.2023.101898.

References

Abdel-Rahman, R.F., Alqasoumi, S.I., Ogaly, H.A., et al., 2020. Propolis ameliorates cerebral injury in focal cerebral ischemia/reperfusion (I/R) rat model via upregulation of TGF-β1. Saudi Pharm. J. 28, 116–126. https://doi.org/10.1016/j.jsps.2019.11.013.

Alatawi, F. S., U. A. Faridi and M. S. Alatawi, 2018. Effect of treatment with vitamin D plus calcium on oxidative stress in streptozotocin-induced diabetic rats. 26, 1208-1213. 10.1016/j.jsps.2018.07.012.

Almarfadi, O.M., Siddiqui, N.A., Shahat, A.A., et al., 2022. Quantification of biomarkers and evaluation of antioxidant, anti-inflammatory, and cytotoxicity properties of *Dodonaea viscosa* grown in Saudi Arabia using HPTLC technique. Open Chem. 20, 559–569. https://doi.org/10.1515/chem-2022-0181.

Althurwi, H.N., Abdel-Rahman, R.F., Soliman, G.A., et al., 2022. Protective Effect of Beta-Carotene against Myeloperoxidase-Mediated Oxidative Stress and Inflammation in Rat Ischemic Brain Injury. Antioxidants. 11, 2344. https://doi.org/10.3390/antiox11122344.

An, L., Zhu, D., Zhang, X., et al., 2022. Isoastilbin inhibits neuronal apoptosis and oxidative stress in a rat model of ischemia-reperfusion injury in the brain: Involvement of SIRT1/3/6. Adv. Clin. Exp. Med. 31, 49–57. https://doi.org/10.17219/acem/142164.

Dai, Y., Zhang, H., Zhang, J., et al., 2018. Isoquercetin attenuates oxidative stress and neuronal apoptosis after ischemia/reperfusion injury via Nrf2-mediated inhibition of

the NOX4/ROS/NF-kappaB pathway. Chem. Biol. Interact. 284, 32–40. https://doi.org/10.1016/j.cbi.2018.02.017.
Fan, S., Liu, X., Wang, Y., et al., 2021. *Thymus quinquecostatus* Celak. ameliorates cerebral ischemia-reperfusion injury via dual antioxidant actions: Activating Keap1/Nrf2/HO-1 signaling pathway and directly scavenging ROS. Phytomedicine 91, 153673. https://doi.org/10.1016/j.phymed.2021.153673.
Faraz, I., Ali, A., Ul Haq, F., et al., 2019. Sensitive Determination of C-Alkylated Flavonoids by HPLC-ESI-MS/MS Using Multiple Reaction Monitoring Approach: Pseudarthria hookeri as a Case Study. J. Chromatogr. Sci. 57, 944–949. https://doi.org/10.1093/chromsci/bmz072.
Fifield, K.E., Vanderluit, J.L., 2020. Rapid degeneration of neurons in the penumbra region following a small, focal ischemic stroke. Eur. J. Neurosci. 52, 3196–3214. https://doi.org/10.1111/ejn.14678.
Gupta, S., Upadhayay, D., Sharma, U., et al., 2018. Citalopram attenuated neurobehavioral, biochemical, and metabolic alterations in transient middle cerebral artery occlusion model of stroke in male Wistar rats. J. Neurosci. Res. 96, 1277–1293. https://doi.org/10.1002/jnr.24226.
Heidari, Z., Mahmoudzadeh-Sagheb, H., Sarbishegi, M., et al., 2021. *Withania coagulans* extract attenuates oxidative stress-mediated apoptosis of cerebellar purkinje neurons after ischemia/reperfusion injury. Metab. Brain Dis. 36, 1699–1708. https://doi.org/10.1007/s11011-021-00745-0.
Hossain, M.A., 2019. Biological and phytochemicals review of Omani medicinal plant. J. King Saud. Univ. Sci. 31, 1089–1094. https://doi.org/10.1016/j.jksus.2018.09.012.
Huang, J., Chen, L., Yao, Z.M., et al., 2023. The role of mitochondrial dynamics in cerebral ischemia-reperfusion injury. Biomed. Pharmacother. 162, 114671 https://doi.org/10.1016/j.biopha.2023.114671.
Ilhan, M., Ali, Z., Khan, I.A., et al., 2019. Bioactivity-guided isolation of flavonoids from *Urtica dioica* L. and their effect on endometriosis rat model. J. Ethnopharmacol. 243, 112100 https://doi.org/10.1016/j.jep.2019.112100.
Jelinek, M., Jurajda, M., Duris, K., 2021. Oxidative Stress in the Brain: Basic Concepts and Treatment Strategies in Stroke. Antioxidants. 10, 1886. https://doi.org/10.3390/antiox10121886.
Jittiwat, J., Chonpathompikunlert, P., Sukketsiri, W., 2021. Neuroprotective effects of *Apium graveolens* against focal cerebral ischemia occur partly via antioxidant, anti-inflammatory, and anti-apoptotic pathways. J. Sci. Food Agric. 101, 2256–2263. https://doi.org/10.1002/jsfa.10846.
Kamal, F.Z., Lefter, R., Jaber, H., et al., 2023. The Role of Potential Oxidative Biomarkers in the Prognosis of Acute Ischemic Stroke and the Exploration of Antioxidants as Possible Preventive and Treatment Options. Int. J. Mol. Sci. 24, 6389. https://doi.org/10.3390/ijms24076389.
Khan, K., Rasool, S., Khan, K., et al., 2019. Computational Evaluation and Anti-inflammatory and Analgesic Activities of Nebrodenside A Isolated From *Dodonaea viscosa*. Nat. Prod. Commun. 14 https://doi.org/10.1177/1934578X19848157.
Lan, B., Ge, J.W., Cheng, S.W., et al., 2020. Extract of Naotaifang, a compound Chinese herbal medicine, protects neuron ferroptosis induced by acute cerebral ischemia in rats. J. Integr. Med. 18, 344–350. https://doi.org/10.1016/j.joim.2020.01.008.
Liang, H., Chang, X., Xia, R., et al., 2022. Magnoflorine Attenuates Cerebral Ischemia-Induced Neuronal Injury via Autophagy/Sirt1/AMPK Signaling Pathway. Evid. Based Complement. Alternat. Med. 2022, 2131561. https://doi.org/10.1155/2022/2131561.
Nandi, A., Yan, L.-J., Jana, C.K., et al., 2019. Role of Catalase in Oxidative Stress- and Age-Associated Degenerative Diseases. Oxid. Med. Cell. Longev. 2019, 9613090. https://doi.org/10.1155/2019/9613090.
Otify, A.M., El-Sayed, A.M., Michel, C.G., et al., 2019. Metabolites profiling of date palm (Phoenix dactylifera L.) commercial by-products (pits and pollen) in relation to its antioxidant effect: a multiplex approach of MS and NMR metabolomics. Metabolomics 15, 119. https://doi.org/10.1007/s11306-019-1581-7.
Owolabi, M.O., Thrift, A.G., Mahal, A., et al., 2022. Primary stroke prevention worldwide: translating evidence into action. Lancet Public Health 7, e74–e85. https://doi.org/10.1016/S2468-2667(21)00230-9.
Peng, T., Jiang, Y., Farhan, M., et al., 2019. Anti-inflammatory Effects of Traditional Chinese Medicines on Preclinical in vivo Models of Brain Ischemia-Reperfusion-Injury: Prospects for Neuroprotective Drug Discovery and Therapy. Front. Pharmacol. 10, 204. https://doi.org/10.3389/fphar.2019.00204.
Perna, R., Temple, J., 2015. Rehabilitation outcomes: ischemic versus hemorrhagic strokes. Behav. Neurol. 2015, 1–6. https://doi.org/10.1155/2015/891651.
Raj, S., C. Bhattacharyya, A. Sarkar, et al., 2021. Glutathione: role in oxidative/nitrosative stress, antioxidant defense, and treatments. ChemistrySelect. 6, 4566-4590. 0.1002/slct.202100773.
Salinas-Sánchez, D.O., Zamilpa, A., Pérez, S., et al., 2015. Effect of Hautriwaic Acid Isolated from *Dodonaea viscosa* in a Model of Kaolin/Carrageenan-Induced Monoarthritis. Planta Med. 81, 1240–1247. https://doi.org/10.1055/s-0035-1546197.
Sarkar, S., Chakraborty, D., Bhowmik, A., et al., 2019. Cerebral ischemic stroke: cellular fate and therapeutic opportunities. FBL. 24, 415–430. https://doi.org/10.2741/4727.
Shah, M.A., Kang, J.B., Park, D.J., et al., 2021. Chlorogenic acid alleviates neurobehavioral disorders and brain damage in focal ischemia animal models. Neurosci. Lett. 760, 136085 https://doi.org/10.1016/j.neulet.2021.136085.
Shi, Y.-J., Sun, L.-L., Ji, X., et al., 2021. Neuroprotective effects of oleanolic acid against cerebral ischemia-reperfusion injury in mice. Exp. Neurol. 343, 113785 https://doi.org/10.1016/j.expneurol.2021.113785.
Shou, J.W., Li, X.X., Tang, Y.S., et al., 2022. Novel mechanistic insight on the neuroprotective effect of berberine: The role of PPARdelta for antioxidant action. Free Radic. Biol. Med. 181, 62–71. https://doi.org/10.1016/j.freeradbiomed.2022.01.022.
Siddiqui, N.A., Almarfadi, O.M., Shahat, A.A., et al., 2023. Isolation of new compound and neuroprotective studies from *Dodonaea viscosa*. J King Saud Univ Sci. 35, 102704 https://doi.org/10.1016/j.jksus.2023.102704.
Tseuguem, P.P., Ngangoum, D.A.M., Pouadjeu, J.M., et al., 2019. Aqueous and methanol extracts of Paullinia pinnata L. (Sapindaceae) improve inflammation, pain and histological features in CFA-induced mono-arthritis: Evidence from in vivo and in vitro studies. J. Ethnopharmacol. 236, 183–195. https://doi.org/10.1016/j.jep.2019.02.048.
Wang, Y., Wang, M.D., Xia, Y.P., et al., 2018. MicroRNA-130a regulates cerebral ischemia–induced blood–brain barrier permeability by targeting Homeobox A5. FASEB J. 32, 935–944. https://doi.org/10.1096/fj.201700139RRR.
Zhang, X., Han, B., Feng, Z.-M., et al., 2017. Phthalide derivatives from *Ligusticum chuanxiong*. RSC Adv. 7, 37478–37486. https://doi.org/10.1039/C7RA06813A.
Zhang, L.-B., Ji, J., Lei, C., et al., 2012. Isoprenylated Flavonoid and Adipogenesis-Promoting Constituents of *Dodonaea viscosa*. J. Nat. Prod. 75, 699–706. https://doi.org/10.1021/np2009797.
Zhang, Y., Zhang, Z., Wang, J., et al., 2022. Scutellarin alleviates cerebral ischemia/reperfusion by suppressing oxidative stress and inflammatory responses via MAPK/NF-κB pathways in rats. Environ. Toxicol. 37, 2889–2896. https://doi.org/10.1002/tox.23645.